Variational Inversion of the SSM/I Observations during the ASTEX Campaign

C. PRIGENT*

Département de Radioastronomie Millimétrique, CNRS, Observatoire de Paris, Paris, France

L. PHALIPPOU

European Centre for Medium-Range Weather Forecasts, Reading, United Kingdom

S. ENGLISH

Satellite Applications Section, Numerical Weather Prediction Division, U.K. Meteorological Office, Bracknell, United Kingdom

(Manuscript received 1 February 1996, in final form 26 September 1996)

ABSTRACT

Given the prospect of direct assimilation of satellite microwave radiances within numerical weather prediction (NWP) schemes, this study proposes to test a nonlinear inversion for retrieving geophysical parameters from Special Sensor Microwave/Imager (SSM/I) measurements using NWP forecasts as a priori information. The inversion method relies upon an accurate analysis of the radiative transfer and simultaneously retrieves the surface wind speed, the integrated water vapor, and the cloud liquid water.

The method is tested in the framework of the well-documented Atlantic Stratocumulus Transition Experiment campaign. The validation approach involves radiosondes from islands, ships, and drifting buoys, cloud liquid water measurements from instruments onboard the U.K. Meteorological Office C-130 aircraft, and the International Satellite Cloud Climatology Project cloud liquid water estimates. The retrieved geophysical parameters are in satisfactory agreement with the available in situ measurements, and the inversion process is shown to be reliable even in the detection of low liquid water contents.

The SSM/I inversion scheme is also a strategy for the validation of radiative transfer models, the discrepancy between the simulated and the observed radiances at the end of the inversion process being a powerful tool for testing the radiative transfer in use.

1. Introduction

The Defense Meteorological Satellite Program (DMSP) satellites observe the earth twice daily, with near-polar, circular, sun-synchronous orbits. The Special Sensor Microwave/Imager (SSM/I) onboard DMSP satellites has seven channels, which sense atmospheric and surface emissions between 19 and 85 GHz (Hollinger et al. 1987). Several statistical or semistatistical algorithms have been developed to retrieve the sea surface wind speed (WS), integrated water vapor content (WV), and cloud liquid water path (LWP) from SSM/I measurements (Goodberlet et al. 1989; Alishouse et al. 1990a,b, among others; see Hollinger 1991 for a review). These satellite products provide an improved description of the horizontal structure of the atmospheric fields, compared to radiosondes or buoys. Recent assimilation experiments of WV satellite estimates in research numerical weather prediction (NWP) models show a positive impact on the forecast (Kuo et al. 1993; Filiberti et al. 1994). In addition, while radiosondes do not provide access to cloud parameters, and IR or optical satellite observations only penetrate the top of the clouds, microwave measurements offer the capability of measuring the whole cloud liquid water path over the whole globe. Currently, several NWP models include schemes to calculate cloud amount from NWP model variables, but in order to introduce the cloud physics into the models and calculate the cloud radiative properties, an estimation of the cloud water content is needed as an input into the model (Smith 1990).

However, in the presence of cloud, the SSM/I statistical algorithms undergo some difficulties. They have problems accounting for the variability of all the related parameters, and they do not properly handle the nonlinearity of the inversion problem. The sensitivity of the SSM/I radiances to parameters such as the sea surface temperature or the temperature profile is too weak for

*Current affiliation: Columbia University, NASA/Goddard Institute for Space Studies, New York, New York.

Corresponding author address: Dr. C. Prigent, NASA/Goddard Institute for Space Studies, New York, NY 10025.
E-mail: cprigent@giss.nasa.gov

retrieving these parameters. Therefore, these parameters need to be known a priori to reduce the noise in the retrieval. In an ordinary regression method, the background takes the form of a climatological profile that can exhibit a large discrepancy with the real atmospheric state and yield significant retrieval errors in the SSM/I-derived geophysical parameters.

NWP assimilation schemes were historically developed to use radiosonde data, and for assimilation within NWP models, satellite data were first inverted to retrieve temperature and humidity parameters and then assimilated as radiosonde data. This results in high-quality satellite radiance measurements being treated as poor-quality radiosondes, which led to a negative impact in some regions when satellite-derived products were first introduced to NWP schemes. Efforts today are being directed toward direct assimilation of the satellite radiances or brightness temperatures rather than toward the related retrieved geophysical products, provided that the radiative transfer associated with these measurements is accurate enough (Eyre 1989; Eyre at al. 1993). Satellite retrievals and NWP assimilations are very similar mathematical inverse problems than can be jointly solved with benefits. When merging the inversion of the satellite data into the NWP scheme, one profits from the atmospheric information already available by means of the NWP forecast with its associated error. The background information derived from the NWP forecast is expected to be much closer to the real atmospheric state than the global climatologies usually used in statistical algorithms. In addition, within an NWP procedure, one naturally handles the nonlinearity of the inversion problem by using the variational method adopted in the assimilation scheme. This procedure is already successfully used by the Television Infrared Observation Satellite (TIROS) Operational Vertical Sounder (TOVS) for temperature and humidity profile retrievals (Eyre et al. 1993).

A nonlinear inversion has already been applied to SSM/I observations during a North Atlantic cyclone (Prigent et al. 1994). Recently, the first step toward the direct assimilation of SSM/I radiances into the NWP system has been described by Phalippou (1996). In this study, we propose to use a similar method and to test it in comparison with in situ measurements. The inversion process is validated with the help of the high-quality measurements performed during the Atlantic Stratocumulus Transition Experiment (ASTEX) experimental campaign over the Azores in June 1992. The validation strategy involves radiosondes from islands and ships, wind measurements from drifting buoys and ships, liquid water measurements from onboard an aircraft within clouds, and the International Satellite Cloud Climatology Project (ISCCP) cloud liquid water estimates. In section 2, the inversion procedure is presented, with emphasis on the radiative transfer used in the scheme, and the information derived from the ECMWF (European Centre for Medium-Range Weather Forecasts) forecasts is described. The ASTEX in situ measurements used in this study are described in section 3. The inversion procedure is applied to the *F10* and *F11* SSM/I observations, in coincidence with in situ measurements. The results are presented and compared to the in situ measurements and to ''classical'' SSM/I regression algorithms (section 4). The sensitivity of the retrieval to the radiative transfer model is discussed. Section 5 concludes this study.

2. A physically based inversion scheme

a. The inversion method

The scheme performs a nonlinear inversion of the SSM/I measurements to simultaneously retrieve physically consistent estimates of the surface wind speed, integrated water vapor content, and cloud liquid water path. It is derived from the Newtonian nonlinear iterative method described by Rodgers (1976) and Eyre (1989). As the inversion problem is mathematically ill conditioned, several combinations of the variables to be determined may be consistent with the measurements, unless additional constraints are used. These further constraints take the form of a first-guess estimate associated with their error covariances. The maximum probability solution will minimize the following cost function:

$$\chi(\mathbf{x})^2 = [\mathbf{y}_{\text{obs}} - \mathbf{y}(\mathbf{x})]^{\mathrm{T}}\mathbf{E}^{-1}[\mathbf{y}_{\text{obs}} - \mathbf{y}(\mathbf{x})] + (\mathbf{x}_b - \mathbf{x})^{\mathrm{T}}\mathbf{C}^{-1}(\mathbf{x}_b - \mathbf{x}), \quad (1)$$

where $\mathbf{x}$ is a vector representing the atmospheric variables to be estimated; $\mathbf{y}(\mathbf{x})$ is the vector of SSM/I brightness temperatures simulated with a forward radiative transfer model and corresponding to the atmospheric state $\mathbf{x}$; $\mathbf{y}_{\text{obs}}$ is the vector of the measured SSM/I brightness temperatures; $\mathbf{E}$ is the matrix representing the channel noise variances—that is, the noise due to the instrument and the radiative transfer model; $\mathbf{x}_b$ is the vector describing the first-guess geophysical state, with $\mathbf{C}$ being the error covariance matrix associated to it; and superscripts T and -1 correspond to the matrix transpose and inverse, respectively.

To find the maximum probability solution of $\mathbf{x}$, Eq. (1) is minimized; that is, assuming there are no multiple minima, the gradient of $\chi(\mathbf{x})^2$ with respect to $\mathbf{x}$ is set to zero:

$$0 = -\mathbf{K}(\mathbf{x})^{\mathrm{T}}\mathbf{E}^{-1}[\mathbf{y}_{\text{obs}} - \mathbf{y}(\mathbf{x})] + \mathbf{C}^{-1}(\mathbf{x}_b - \mathbf{x}), \quad (2)$$

with $\mathbf{K}(\mathbf{x})$ containing the partial derivative of $\mathbf{y}(\mathbf{x})$ with respect to the elements of $\mathbf{x}$.

Then, the Newtonian method consists of expanding the brightness temperature vector $\mathbf{y}$ as a Taylor series about a guessed value $\mathbf{x}_n$:

$$\mathbf{y}(\mathbf{x}) = \mathbf{y}(\mathbf{x}_n) + \mathbf{K}(\mathbf{x}_n)(\mathbf{x} - \mathbf{x}_n). \quad (3)$$

It yields

$$\mathbf{x}_{n+1} = \mathbf{x}_n + [\mathbf{C}^{-1} + \mathbf{K}(\mathbf{x}_n)^{\mathrm{T}}\mathbf{E}^{-1}\mathbf{K}(\mathbf{x}_n)]^{-1} \times [\mathbf{K}(\mathbf{x}_n)^{\mathrm{T}}\mathbf{E}^{-1}[\mathbf{y}_{\mathrm{obs}} - \mathbf{y}(\mathbf{x}_n)] + \mathbf{C}^{-1}(\mathbf{x}_{\mathrm{b}} - \mathbf{x}_n)]. \quad (4)$$

The error covariance of the nth guess is given by

$$\mathbf{S}(\mathbf{x}_n) = [\mathbf{C}^{-1} + \mathbf{K}(\mathbf{x}_n)^{\mathrm{T}}\mathbf{E}^{-1}\mathbf{K}(\mathbf{x}_n)]^{-1}. \quad (5)$$

Here, $\mathbf{S}(\mathbf{x}_n)$ is an estimate of the error covariance of the solution for the step n (Rodgers 1976). For the final vector $\mathbf{x}$ and the corresponding $\mathbf{K}(\mathbf{x})$, the matrix $\mathbf{S}$ is an estimate of the error covariance of the retrieval.

Within the iterative process, the geophysical variables to be retrieved have to keep meaningful values (essentially they should not turn negative). The NAG procedure E04LBF (NAG 1991) has been adopted here; it is based on the Newtonian method and is suitable for finding the minimum of a function with variables subject to fixed bounds (Phalippou 1996).

b. The radiative transfer and the SSM/I channels

Within the inversion procedure, the radiative transfer model has to be accurate enough to give a good estimate of the brightness temperatures, and of the first derivatives of the brightness temperatures with respect to all the geophysical parameters and for all the frequencies. It is worth remembering here that this need for an accurate radiative transfer model also applies when developing SSM/I algorithms from a statistical regression of simulated brightness temperatures against atmospheric and surface parameters.

The key features of the radiative transfer are presented in section 2b(1), and the sensitivity of the SSM/I channels to the geophysical parameters is analyzed in section 2b(2). The SSM/I channel errors are discussed in section 2b(3).

1) THE RADIATIVE TRANSFER MODEL

(i) The gaseous absorption model

The MPM93 (Millimeter-Wave Propagation Model) gaseous absorption model of Liebe et al. (1993) is adopted for all the SSM/I frequencies. In this model, H_2O and O_2 lines are added up to 1 THz, assuming a Van Vleck Weisskopf line shape. For the oxygen, this function was modified by Rosenkranz (1992) to include line coupling in the 60-GHz band. An empirical H_2O continuum is added, derived from laboratory measurements. Although Ma and Tipping (1990) proposed a theoretical explanation for this phenomenon, the behavior of the H_2O absorption in the gaps between the lines is still a debatable point and experimental efforts are still being carried out, both in laboratories and in the atmosphere, to gain accuracy in the estimation of this so-called continuum (Westwater et al. 1990; Walter 1992; Bauer et al. 1993; Han et al. 1994; English et al. 1994).

(ii) The cloud contribution

Only the subtropical North Atlantic marine atmosphere is examined in this study. In this area, the stratocumulus drops are generally small, with typical effective radii of 12 μm, and up to 90 GHz we can assume that the total extinction coefficient of the cloud is close to the absorption coefficient and that the scattering process is neglected. The cloud temperature is assumed to be equal to the air temperature. The dielectric properties of liquid water stem from Manabe et al. (1987). The stratocumulus clouds are free of ice in the Azores area in June. Even when cirrus clouds are present, they do not contribute significantly to the brightness temperatures (this has been confirmed by upward microwave observations onboard the C-130 of the U.K. Meteorological Office; see English 1995). No rain cases were encountered during this study.

(iii) The sea surface model

For the sea surface contribution, a geometric optics approach (Prigent and Abba 1990) is adopted, derived from Wilheit (1979). The ocean surface is described as a set of reflecting plane surfaces characterized by a bidirectional slope distribution. Each individual facet is assumed to be infinite in size in front of the wavelength, and irregularities that are small compared to the wavelength are ignored. The elementary contribution of each facet is computed from Fresnel's reflection laws. The surface scattering component of the brightness temperatures results from the integration of the atmospheric radiation over the whole upper hemisphere. The dielectric properties of the seawater are calculated from Klein and Swift (1977). The slope distribution is given by Cox and Munk (1954) as a function of the wind speed measured at an altitude of 12.5 m above the surface. The shape of the distribution is Gaussian, slightly modified to account for the upwind–downwind asymmetry. Shadowing and multiple reflection effects are taken into account. In the presence of foam, for each facet, the apparent temperature is modified by including a foam coverage (following Wu 1979) with a foam emissivity of one. For a thorough discussion of this model, see Guillou et al. (1996).

2) THE SENSITIVITY OF THE SSM/I CHANNELS TO THE GEOPHYSICAL PARAMETERS

The SSM/I has seven channels at 19.35, 22.235, 37.0, and 85.5 GHz, for both vertical and horizontal polarizations, except for 22.235 GHz, which is only observed in vertical polarization. The observing incident angle on the earth is close to 53°, and the fields of view decrease proportionally with the frequency from 60 × 43, to 40 × 50, to 28 × 37, to 13 km × 15 km. The seven channel brightness temperatures are used in this study at their nominal resolutions—that is, without attempting any matching of the different spatial resolutions.

The SSM/I channel sensitivity to the main geophysical parameters of interest (the wind speed, integrated water vapor, and cloud liquid water path) are presented in Fig. 1. For a given frequency, the horizontal polarization of the signal is always more sensitive to the geophysical parameters because of the lower emissivity of the ocean surface for this polarization, which gives higher thermal contrast with the atmosphere. Although situated in an H_2O line, the 22.235-GHz channel has a similar sensitivity to the water vapor compared to the 85-GHz channel, but its sensitivity to the water vapor does not depend on the cloud liquid water content. Figure 1d illustrates the ability of the 85-GHz channel to detect low cloud liquid water contents; however for higher cloud liquid water, the 85-GHz channel saturates and the 37-GHz channel provides most information. For low liquid water content, the radiometric effects of vapor and droplets at all frequencies are very similar, except at 22 GHz. Because of their selective sensitivity to the various parameters, the seven channels are used in the inversion process. Figure 1 clearly shows that in the presence of clouds the problem becomes nonlinear, such that an iterative inversion process is required, involving the explicit calculation of the radiative transfer parameters at each step.

In this study, the geophysical parameters to be retrieved are the WS, WV, and LWP. Although the SSM/I observations have been shown to be slightly sensitive to the humidity structure in the lower atmosphere (see Petty 1990; Phalippou 1996, among other authors), this effect will be neglected here, and only the integrated humidity will be considered in the inversion process.

All the parameters to be retrieved interact with the traveling electromagnetic waves to a comparable amplitude for several SSM/I frequencies. Gagarin and Kutusa (1983) concluded from simulations that ambiguity on the surface roughness can yield important errors in the estimation of water vapor and liquid vapor estimates. From an error analysis, Greenwald et al. (1993) confirmed that the retrieval errors in cloud liquid water content vary depending on the errors in the surface and atmospheric conditions, with the surface conditions being an important factor for low cloud liquid water contents. By comparing the ISCCP products with SSM/I cloud liquid retrieval, Lin and Rossow (1994) noted that errors in water vapor contents can produce errors in cloud liquid water as large as 0.3 kg m^{-2} in tropical areas. When retrieving all the parameters simultaneously, with a constraint on the ECMWF a priori information, one verifies that the set of retrieved parameters jointly satisfies the minimization of Eq. (1), and the estimation error on each parameter is minimized.

3) THE SSM/I CHANNEL NOISE

The channel noise standard deviations [matrix **E** in Eq. (1)] include not only the instrumental noise, which amounts to 0.5 K, but also noise arising from errors in the radiative transfer model, unmodeled geophysical contributions to the brightness temperatures, and inhomogeneities in the scenes. A standard deviation of 2 K is adopted for the five lower-frequency channels and 3 K for the 85.5-GHz channels (Petty 1990; Phalippou 1996). Mainly because of the cloud beam filling problem, the weight of the 85-GHz channel in the retrieval is set lower than those for the other channels. The channel errors are assumed to be uncorrelated between channels, leading to a diagonal **E** matrix.

c. The ECMWF a priori information and the associated constraints

In the framework of NWP assimilations, whichever SSM/I retrieval method is adopted, the SSM/I-retrieved products will eventually be combined with the NWP data. The method we propose makes use of the prior knowledge of the atmosphere provided by the NWP forecast. The ECMWF forecast fields are selected to be the first-guess atmospheric state in the inversion process; that is, the ECMWF information gives an estimation of the atmospheric state $\mathbf{x}_1$ in Eqs. (1)–(3), from which the first set of simulated SSM/I radiances are calculated [$\mathbf{y}(\mathbf{x}_1)$]. The ECMWF information we use includes the temperature and water vapor profiles, the surface temperature, and the sea surface wind speeds. The ECMWF forecast fields used in this study have a horizontal resolution of 62 km and the atmosphere is sampled on 31 levels between the surface and 10 mb. They are available every 6 h each day (at 0000, 0060, 1200, and 2400 UTC). For each in situ observation coincident with SSM/I measurements, the background atmospheric parameters are obtained by interpolating in time and space the ECMWF forecasts that surround the observation (see Phalippou 1996). A cloud density of 0.1 g m^{-3} is associated with every atmospheric layer with more than 90% relative humidity and a temperature higher than 253 K. The cloud temperature is assumed to be equal to the air temperature at the same level given by the ECMWF forecast. Although crude, our first estimation of the cloud guarantees that the cloud structure is consistent with the humidity and temperature profile, and will thereby reduce the errors in the cloud estimates. In this study, we could not use the cloud prognostic information recently available in the ECMWF forecast because in 1992 only diagnostic cloud estimations were derived, and these were not archived.

An objective way to select which parameters should be included in the control variable **x** is to analyze the information content of the radiances with respect to those parameters. This can be achieved, for instance, by comparing the a priori error covariance matrix **C** with the a posteriori error covariance matrix **S** (see Phalippou 1996). Here, the control variable contains the wind speed, the total precipitable water, and the cloud liquid water path.

For the variable to be retrieved, the matrix **C** contains

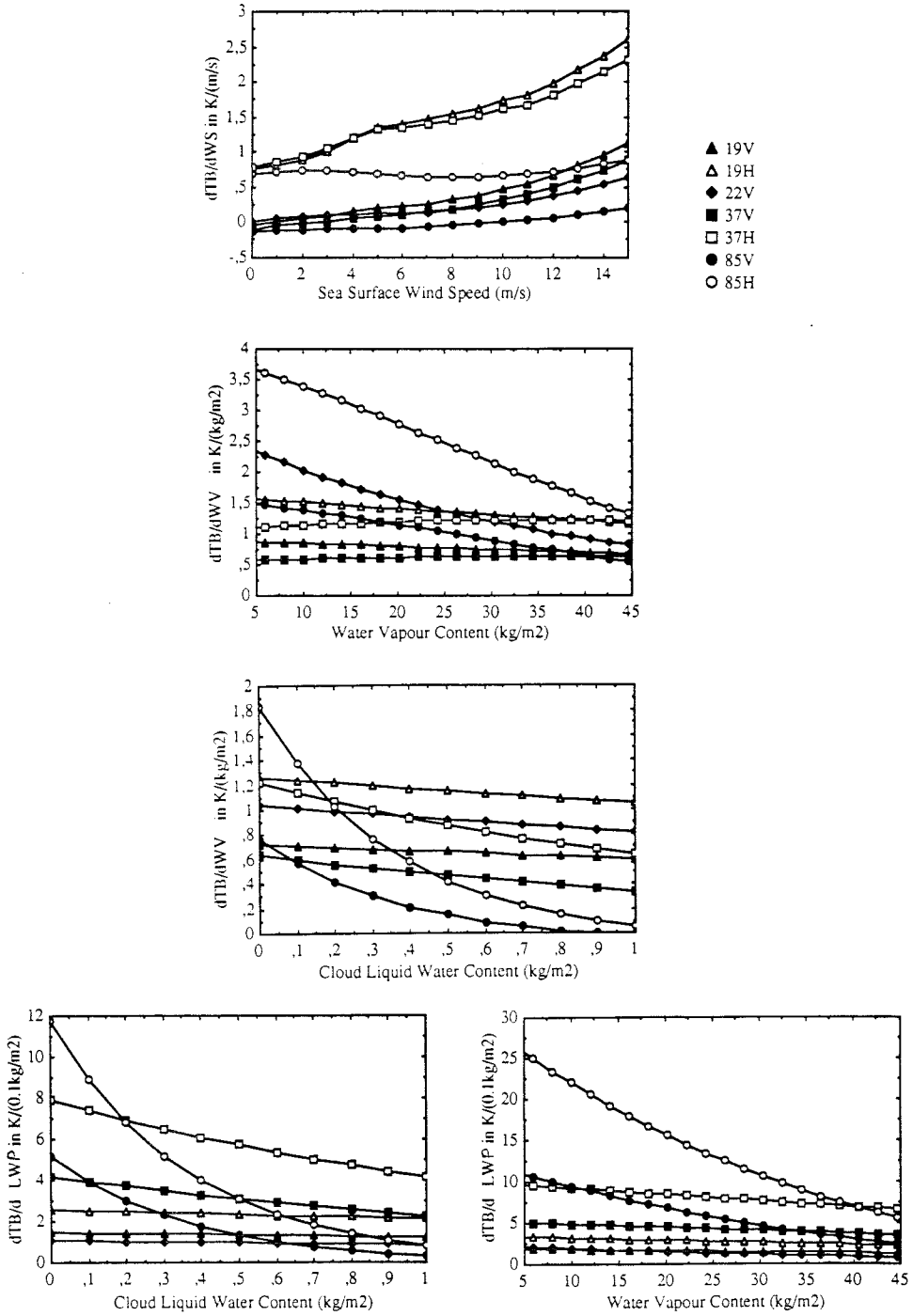

FIG. 1. The sensitivity of the SSM/I brightness temperatures to the main geophysical parameters of interest. (a) Sensitivity to the sea surface wind speed (dTB/dWS) as a function of wind speed, (b) sensitivity to the water vapor content (dTB/dWV) as a function of the water vapor content and (c) as a function of the cloud liquid water content, and (d) sensitivity to the cloud liquid water content (dTB/dLWP) as a function of the cloud liquid water path and (e) as a function of the water vapor content. The sea surface temperature is set at 297 K. The water vapor scale height is 2 km, with an effective temperature lapse rate of 6.5 km. When not specified, the integrated water vapor content is set to 35 kg m^{-2}, the wind speed to 7 m s^{-1}, and the cloud liquid water content to 0 kg m^{-2}. When present, the cloud sits between 800 and 1500 m. Here, (a) and (b) correspond to cloud-free atmospheres. For (e) the sensitivity of the cloud liquid water content is calculated around 0.1 kg m^{-2}.

the error covariance associated with the a priori information. The error background on the wind speed is set to 2 m s^{-1}, which corresponds to a rather strong constraint. This reflects both the level of confidence we have in the ECMWF wind fields (Stoffelen and Anderson 1994) and our doubts in the ability of the SSM/I to retrieve wind speed in the case of deep clouds. For each ECMWF atmospheric profile, the error covariance of the integrated water vapor is calculated from the error covariance on each humidity level given by Eyre et al. (1993) for the TOVS processing. The error covariance varies between 4 and 18 kg m^{-2}, respectively, for atmospheres of 10 and 45 kg m^{-2}. The error covariance on the LWP is set to 0.2 kg m^{-2} in order to encompass a broad population of clouds. It represents a weak constraint that allows for the lack of reliable a priori cloud information.

During the inversion process, for each SSM/I pixel, the initial atmospheric parameters (WS, WV, and LWP) are modified iteratively until there is a satisfactory minimization of Eq. (1). The water vapor density in each layer of the initial ECMWF profile is uniformly scaled for the atmospheric profile to fit the integrated water vapor content imposed during the inversion process. In each layer, water vapor contents exceeding saturation are truncated and are compensated by adding water vapor to adjacent layers. Within the cloud, the liquid water content is assumed constant with altitude and is scaled to match the LWP dictated by the inversion.

3. The ASTEX campaign: Satellite observations and in situ measurements

The ASTEX campaign took place in the Azores area in June 1992. Its main objective was to aid in the development of physical parameterizations in the stratocumulus regimes for numerical models. This subtropical region is of great importance for the heat balance of the ocean. The marine stratocumulus clouds in these areas have a high albedo that reduces the flux of solar energy into the ocean, while because of their low altitude, these clouds do not appreciably change the outgoing longwave radiations—the loss of solar energy in the atmospheric column is not compensated by reduced longwave emission to space. ASTEX was proposed to establish an adequate observation database to improve understanding the physics of these marine clouds.

The experimental setup during the campaign is presented in Fig. 2. This campaign offers high-quality in situ measurements of a large number of geophysical parameters. In addition to the routine radiosonde data and satellite images, it includes observations from ships, aircrafts, and buoys. See Albrecht et al. (1995), and Weill et al. (1995) for a description of the in situ measurements during the ASTEX campaign.

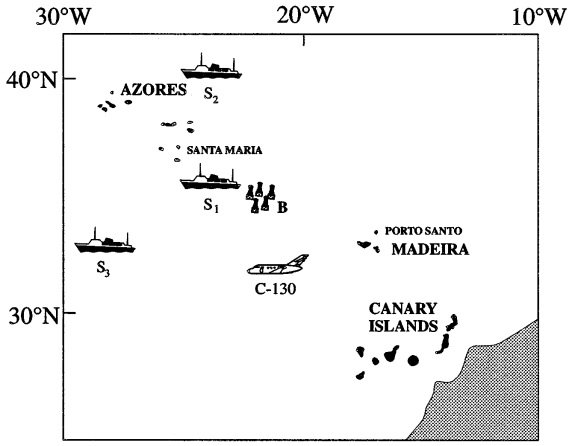

FIG. 2. The experimental setup during the ASTEX campaign in the Azores area in June 1992. Only shown in this figure are the measurement capabilities effectively used in this study; S1 is the ship *Le Suroit,* S2 the *Oceanus,* and S3 the *Malcolm Baldridge.* The five drifting buoys are represented by B. The C-130 aircraft is also indicated.

a. The SSM/I data

The SSM/I data have been collected for both the *F10* and the *F11* DMSP spacecrafts for the whole month of June 1992. The *F11* satellite orbits around the earth with an altitude of 833 km, while the *F10* satellite has an elliptical orbit. For the *F11* spacecraft over the ASTEX area, the morning overpasses occur between 0600 and 0800 UTC, while the evening ones occur between 1700 and 1900 UTC. For the *F10* satellite, the descending orbits take place between roughly 0930 and 1130 UTC, and the ascending orbits between 2045 and 2245 UTC. As the swath of the SSM/I scanning system is 1394 km on the earth with 14.1 orbits per day, at the latitude of the Azores there is not a complete coverage of the ASTEX area twice per day for one satellite, and coincidences between satellite overpasses and in situ measurements are therefore limited in number.

b. The in situ measurements

1) THE RADIOSONDES FROM SHIPS AND ISLANDS

During this campaign, ships navigated with automatic radiosonde stations onboard for temperature, humidity, pressure, and wind profiles. Approximately four soundings were performed per day from each of the following three ships: *Le Suroit,* the *Oceanus,* and the *Malcom Baldridge.* From the islands of Santa Maria, in the Azores, and Madeira (Porto Santo), similar radiosondes were launched. The temperature, humidity, and pressure measurements are of high quality. The errors on the humidity profile are of 10% relative humidity on each atmospheric level. The wind measurements from the radiosondes are not used in this study because they were subject to noise and were frequently of poor quality.

2) THE DRIFTING BUOYS

Five drifting buoys developed by the Centre de Meteorologie Marine (Meteo France) were launched at the beginning of the campaign (Weill et al. 1995). They provided information about the oceanic mixed layer at mesoscale resolution. At the top of the mast of the buoys, 2.5 m above the sea surface, a propeller anemometer measured the wind speed with an accuracy of 1 m s^{-1}. For comparison with satellite-retrieved wind fields, these low-altitude wind speed measurements are extrapolated at 12.5 m using the Charnock's approximation. It is worth noting here that the extrapolation of surface wind speeds from 2.5 m to higher altitude is subject to uncertainties—in the lower-layer atmosphere (below 5 m), the wind speed profile may not be logarithmic, and its behavior can depend on the stability of the atmosphere (among other factors). We can reasonably estimate that the interpolation process increases the measurement error by 20%. Measurements are available every hour and are interpolated at the time of the satellite overpasses.

3) WIND MEASUREMENTS ONBOARD THE FRENCH SHIP *Le Suroit*.

Onboard the ship *Le Suroit*, a sonic anemometer was mounted on the top of a 10-m mast (Weill et al. 1995). The sensor was thus situated at approximately 16.5 m above sea level. The measurements were averaged every 15 min. Throughout the campaign, the sonic system worked well and provided high-quality data, with an accuracy of 1 m s^{-1}. The extrapolation of wind speeds from 16.5 down to 12.5 m (the altitude for which all the wind speeds are compared) is subject to smaller errors than the extrapolation from low-altitude wind speeds up to higher-altitude wind speeds (in the cases of buoys).

4) CLOUD LIQUID WATER MEASUREMENTS ONBOARD THE C-130 OF THE U.K. METEOROLOGICAL OFFICE

Onboard the C-130 of the U.K. Meteorological Office, a Johnson–William hot-wire probe measured the liquid water content within the clouds. The integrated liquid water content was obtained by integrating these measurements with height during an aircraft profile through a cloud. The Johnson–William probe is inefficient at collecting drops with radii greater than 30 μm, but in the case of stratocumulus, the contribution of these drops is negligible. The cloud liquid water contents derived from the Johnson–William probe and the forward-scattering spectrometer probe (FSSP) were in fairly good agreement. For a discussion on the cloud liquid water measurements on board the C-130, see English (1995).

c. The ISCCP cloud estimation

To help analyze the SSM/I LWP spatial structure and to complement the C-130 cloud liquid measurements, the ISCCP data are compared to the SSM/I LWP retrievals. In the ISCCP data, the clouds parameters stem from optical and IR observations provided by a set of polar and geostationary satellites (Rossow and Schiffer 1991). From the visible satellite reflectances, the cloud optical thickness is retrieved, and assuming a cloud drop size distribution with an effective radius of 10 μm, the cloud liquid water path is derived (Lin and Rossow 1994). Based on optical observations, the ISCCP procedure is very effective in the detection of thin clouds. The ISCCP spatial resolution is 30 km.

4. Results and discussion

For the month of June 1992, the inversion process has been applied to the SSM/I observations (*F10* and *F11* data) in collocation with the available in situ measurements. The retrieval is performed for all of the SSM/I pixels situated within 50 km of an in situ measurement. For the wind speed and the water vapor, a distance-weighted mean of the retrieved estimates is calculated for comparison with the in situ measurements. Only the SSM/I pixels over the sea are considered (selected according to the surface flag on the SSM/I datasets).

The performance of the minimization procedure is first discussed in terms of the differences between measured and simulated brightness temperature at the end of the inversion process (section 4a). Then for each variable (WS, WV, and LWP), the retrieved products are compared to the in situ measurements, with emphasis on the sensitivity of the retrieval to the radiative transfer (sections 4b–d).

a. Comparison between measured and simulated radiances at the end of the inversion process

The retrieval performs satisfactorily in most cases, except on some pixels around the islands of Porto Santo in Madeira and Santa Maria in the Azores. This problem was found to be related to a geolocation error of the SSM/I observations—some pixels that were supposed to be over sea were in fact substantially contaminated by the islands.

At the convergence of the inversion process, the difference between the measured and simulated brightness temperatures is a useful diagnostic tool for controlling the quality of the radiative transfer model.

Figure 3 shows the discrepancy between the observations and the simulations for all the channels at the end of the minimization procedure for the 5400 processed pixels. The differences are similar to those found in a frontal situation in a previous work (Prigent et al. 1994). The average discrepancy between the simulated

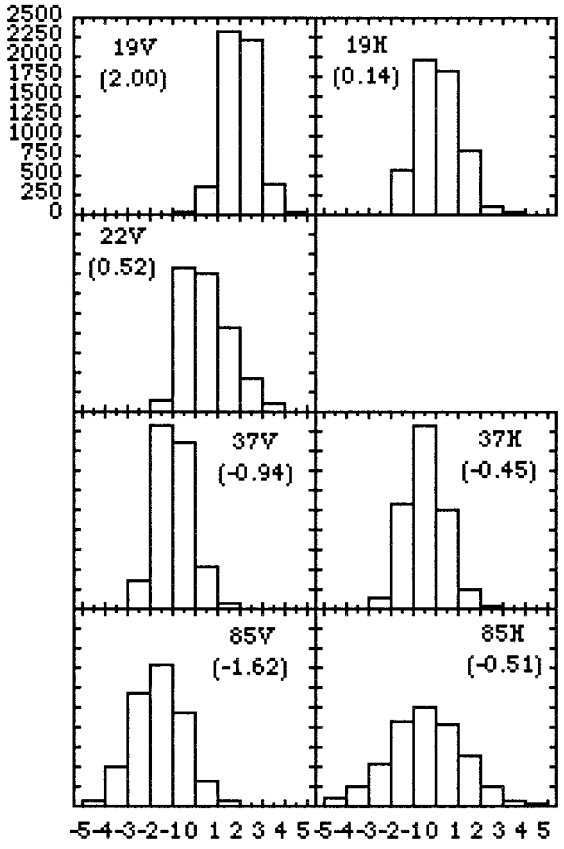

FIG. 3. Histograms of the differences between the observed and simulated brightness temperatures at the end of the inversion process. The mean differences are indicated; 5400 pixels are considered.

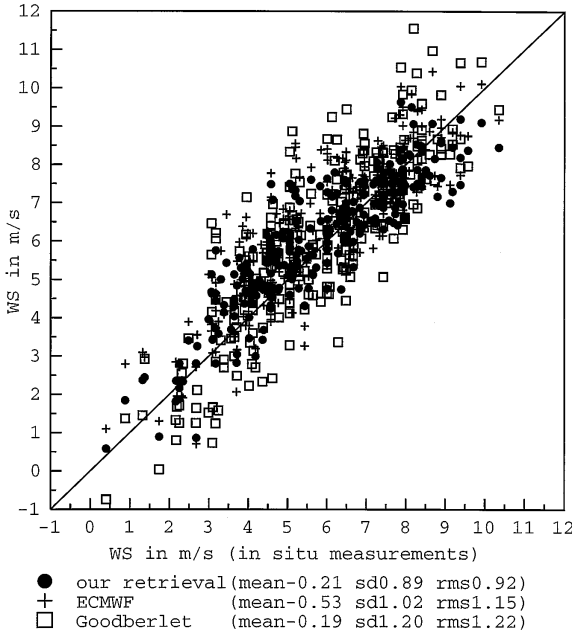

FIG. 4. Comparison of the estimated surface wind speeds with measurements from the five drifting buoys and the mast on the ship *Le Suroit* (282 points). All the winds are extrapolated and compared at 12.5 m. The estimation of Goodberlet et al. (1989) is also displayed.

and the measured brightness temperatures is within the channel noise (2 K for the five lower channels and 3 K for the 85.5-GHz channels). From SSM/I observations and radiative transfer simulations using radiosondes during ICE'89, Karstens et al. (1994) found a similar trend in the mean differences (SSM/I minus model), namely, positive values for the 19- and 22-GHz channels and negative values at 37 GHz, although the amplitude of the discrepancies was larger in the work of Karstens et al. (1994).

In vertical polarization, the 19-GHz channel exhibits an unexplained bias of 2.00 K. The 19-GHz channels are sensitive to the wind speed, but no discrepancy in correlation with wind speed could be demonstrated (at least for the range of wind speeds encountered in this study). The discrepancies at 19 GHz (H and V) are modified when using another sea surface emissivity model within the inversion process. This point will be further discussed in section 4b(2).

b. Wind speed estimations

1) COMPARISON WITH IN SITU MEASUREMENTS

The SSM/I-retrieved wind speeds are compared to the measurements from the five drifting buoys and from the mast on board *Le Suroit* (Fig. 4). The in situ wind speeds do not exceed 11 m s^{-1}. It is worth emphasizing that the in situ measurements correspond to time-averaged wind speeds at a point, while the SSM/I retrievals represent instantaneous spatial averages. The theoretical error on the retrieved wind speed [calculated from Eq. (5) on the 5400 individual processed pixels] has a mean value of 1.24 m s^{-1}, with a standard deviation of 0.11 m s^{-1}. The ECMWF wind speeds and the statistical estimation from Goodberlet et al. (1989) are also shown for comparison. All the winds are extrapolated at an altitude of 12.5 m above the sea surface and are compared at this altitude. The physically based inversion, compared to the in situ measurements, yields an rms error of 0.92 m s^{-1}, with a mean error of -0.21 m s^{-1}. The comparison involves 282 wind measurements. In these cases of clear atmospheres or thin clouds, the performances of our retrieval and of the statistical algorithm are similar, although the statistical method shows a larger rms error.

Whatever the source of in situ measurements (the five buoys or the mast), the scatter in the comparison is comparable. However, for the two satellites, the mean difference between the measurements and the retrievals varies from -0.54 for the *F10* satellite to 0.04 for the *F11* satellite. The same trend is observed for the Goodberlet et al. (1989) retrieval. For the water vapor retrieval, no such dependency has been evidenced (the *F10* and *F11* satellites provide the same statistical results as in situ measurements). This different behavior for the two satellites can be attributed to the *F10* SSM/I

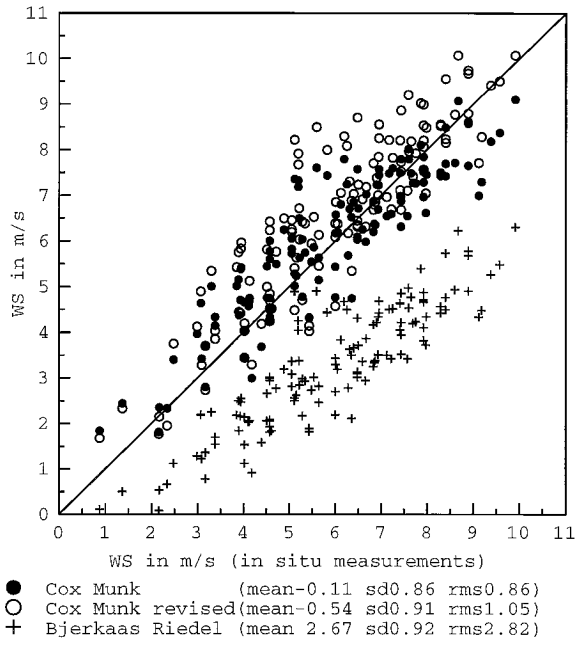

FIG. 5. Comparison of the SSM/I-retrieved surface wind speeds when using the Cox and Munk sea wave spectrum, the Cox and Munk spectrum revised by Wilheit and the Bjerkaas and Riedel spectrum. The comparison is limited to the measurements from two drifting buoys and the mast on *Le Suroit* (130 points).

viewing angle not being perfectly corrected from the ellipticity of the satellite orbit. Around 53°, the sensitivity of the retrieval to scanning geometry is higher for the wind speed than for the water vapor (see Petty 1990), and a small error in the scanning angle for one satellite can explain the observed difference.

2) SENSITIVITY OF THE RETRIEVAL TO THE SEA SURFACE EMISSIVITY MODEL

For the sea surface emissivity, a geometric optics approach has been adopted so far in our retrieval, coupled with the wind-roughened sea surface description of Cox and Munk (1954). However, in the literature, various sea surface descriptions are proposed. For instance, Wilheit (1979) recommends that only a fraction of the slope variances derived by Cox and Munk be considered for frequencies below 37 GHz. As another example, the Bjerkaas and Riedel (1979) wave spectrum and the Cox and Munk sea surface description are both used in the literature, although they differ by a ratio of close to 2 in the associated rms slope. The inversion scheme has been applied to the SSM/I data in coincidence with two buoys and the ship *Le Suroit* for three wave spectra: the Cox and Munk spectrum, the Cox and Munk spectrum revised by Wilheit, and the Bjerkaas and Riedel spectrum. Comparisons of the retrieved wind speeds are presented in Fig. 5. When comparing these three wave spectra using direct radiative transfer simulations against observations, the differences in brightness temperatures are small and difficult to detect. With the Bjerkaas and Riedel spectrum, the retrieved wind speeds strongly underestimate the measurements. The Cox and Munk spectrum revised by Wilheit tends to yield somewhat higher wind speeds and a higher dispersion. In this sense, the inversion process can be seen as a powerful tool for testing the radiative transfer models. For the two wave spectra that have comparable results (the Cox and Munk spectrum and the same spectrum revised by Wilheit), the differences between the simulated and the observed SSM/I temperatures have been compared at the end of the inversion process. The mean difference for each channel is not significantly different, except for channel 19H, which increases and gets closer to the mean discrepancy for channel 19V (as obtained by Phallippou 1996). At that point, the selection of a wave spectrum is a debatable subject, and comparisons are to be extended to other climatological areas before a final conclusion is made.

The sea surface emissivity adapted by Francis et al. (1983) to the SMMR (Scanning Multichannel Microwave Radiometer) measurements has also been tested. It leads to retrieved wind speeds approximately 30% higher than those from the geometric optics model coupled with the Cox and Munk slope distribution. This point is also illustrated by the study of Schluessel and Luthard (1991)—when using the sea surface emissivity model of Francis et al. (1983), the retrieved wind speeds compare badly with in situ measurements.

The sensitivity of the retrieval to the foam model will not be discussed here, although we are convinced that it can influence the retrieval at high wind speeds. But the wind speeds measured during this campaign are too low to induce a significant foam coverage and for any conclusion to be drawn on that point.

The discrepancy between simulations and observations at 19 GHz in horizontal polarization has been investigated in terms of wind directions. A satellite study (Wentz 1992) tends to suggest that the sea surface signal is sensitive to the wind direction. As a consequence, upwind and downwind emissivities would be different, and should be accounted for in the sea surface emissivity simulations. Although the surface slope distribution we use (the Gram Charlier series described by Cox and Munk 1954) accounts for the upwind–downwind asymmetry, the wind direction is not taken into account in our calculation. But, as shown by Wentz (1992) and Phalippou (1996), the sensitivity of the emissivity to the wind direction is primarily significant in H polarization and could not justify the discrepancies at 19 GHz in vertical polarization.

To explain the discrepancies at 19 GHz, the geometric optics treatment itself can also be suspected. Wu and Fung (1972) and Wentz (1975) (among others) have shown that at lower frequencies the geometric treatment was no longer valid, and they found better agreement from the use of two-scale models superimposing small irregularities on the large undulation. However, accord-

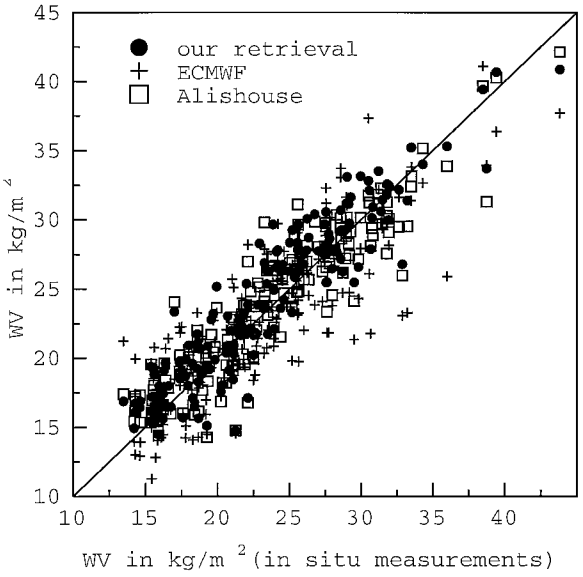

FIG. 6. Comparison of the retrieved integrated water vapor contents with the radiosonde measurements from ships and islands (173 points). The estimation of Alishouse et al. (1990) is also presented for comparison.

ing to these authors, at around 50° incidence the discrepancy between the two-scale models and the geometric approach is much higher in horizontal polarization than in the vertical. We did not test a two-scale model within the inversion process mainly because the uncertainty on the small-scale roughness spectrum is very high—a very small amount of information is available on this spectrum.

c. Water vapor retrieval

1) COMPARISON WITH IN SITU MEASUREMENTS

The retrieved integrated water vapor contents are compared to the radiosonde measurements from ships and islands when the time difference between the radiosondes and the SSM/I overpasses does not exceed 2 h (Fig. 6). The radiosonde values range from 12 to 45 kg m^{-2}. The retrieved products and the measurements are in a good agreement. The theoretical error in the retrieved integrated water vapor [derived from Eq. (5)] has a mean value of 1.43 kg m^{-2}, with a standard deviation of 0.19 kg m^{-2}. Various algorithms available in the literature have also been applied to the SSM/I dataset and compared to the in situ measurements (Alishouse et al. 1990a; Petty and Katsaros 1990; Schluessel and Emery 1990; Bauer and Schluessel 1993). The statistical results (involving 173 comparisons) are presented in Table 1. The algorithms of Alishouse et al. (1990a) and Petty and Katsaros (1990) are derived from a regression analysis based on globally distributed SSM/I matchups with radiosondes. The retrieval coefficients of Schlussel and Emery (1990) and Bauer and Schluessel (1993) are deduced from simulated synthetic brightness temperatures. In this study, the results presented correspond to Schluessel and Emery's algorithm involving three channels [Eq. (6) in their paper] and to Petty and Katsaros's algorithm using three channels. Although derived from independent and different methods, the retrieved water vapor quantities are similar and rather consistent with the in situ measurements, confirming the ability and robustness of the SSM/I channels to estimate the water vapor column, at least in these areas of low liquid water contents. Whatever the retrieval process, the largest dispersion in the differences between retrieved products and in situ measurements were obtained for the island radiosondes (Porto Santo and Santa Maria); contamination of SSM/I pixels by land surfaces is suspected.

TABLE 1. Statistical differences between the integrated water vapor derived from radiosonde measurements and the estimations by various SSM/I water vapor algorithms (the mean, standard deviation, and root-mean-square of the differences are presented). Also presented are the statistical differences between in situ measurements and ECMWF estimates. The comparison involved 173 radiosonde measurements.

	Our retrieval	ECMWF	Alishouse et al. (1990)	Schluessel et al. (1990)	Petty et al. (1990)	Bauer et al. (1993)
Mean	−0.7	0.3	−0.2	1.6	1.2	−1.3
Std. dev.	2.1	3.3	2.3	2.3	2.4	2.4
rms	2.3	3.3	2.3	2.8	2.7	2.7

2) SENSITIVITY OF THE RETRIEVAL TO THE GASEOUS ABSORPTION MODEL

Compared to the MPM89 (Liebe et al. 1989), the MPM93 gaseous absorption model of Liebe et al. (1993) predicts more water vapor absorption. Although the MPM93 agrees better with radiometric observations at 37 and 90 GHz, it still underestimates the lower tail of the 22-GHz water vapor absorption line (Han et al. 1994; Guillou et al. 1993). In the retrieval process, an underestimation of the water vapor gaseous absorption consequently yields an overestimation of the integrated water vapor content and vice versa. The inversion process has been applied with the MPM89 model, and the retrieved products are presented in Fig. 7 compared to the MPM93 products. For this dataset, the MPM93 model is superior to the MPM89. As already stressed, the MPM93 model underestimates the water vapor absorption at 20.6 GHz, in the lower wing of the H_2O line. But it is dangerous to predict the behavior of a model from the wing to the center of the line—MPM93 may be suitable in the center of the line even if it fails in the wings. This study seems to favor the MPM93 model, at least for SSM/I frequencies. However, this conclusion should not be extended to other frequencies (e.g., to the Advanced Microwave Sounding Unit frequencies) without further study.

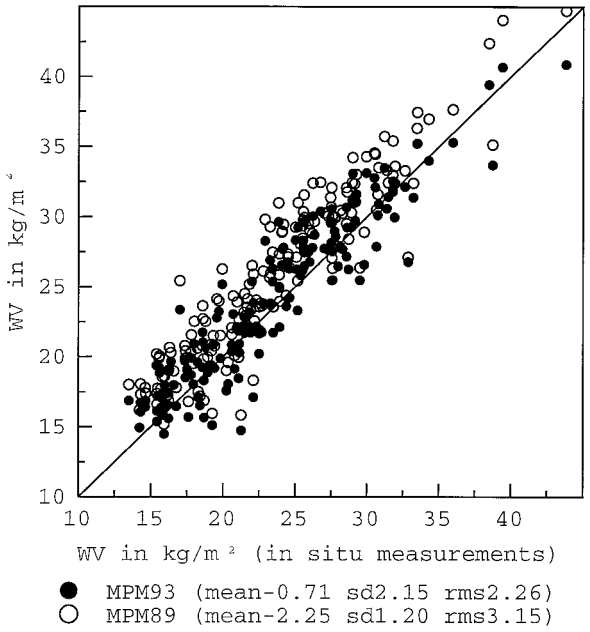

FIG. 7. Comparison of the SSM/I-retrieved integrated water vapor contents when using the MPM89 or the MPM93 models of Liebe et al. (1993) (173 points).

d. Liquid water retrievals

For the 5400 processed pixels, the liquid water path has been retrieved, showing moderate liquid water contents during the whole campaign (maximum of 0.4 kg m^{-2}). The theoretical accuracy of the LWP retrieval is of 0.025 kg m^{-2} in these cases of thin, low, and nonprecipitating clouds.

Direct validation of the liquid water retrieval is hard to perform because cloud liquid water content is not a routinely measured product. Direct measurements of cloud liquid water contents imply the use of a specific instrumentation onboard an aircraft. These measurements are only possible during specific experiments. During the 16 C-130 sorties of ASTEX, cloud profiles were measured and processed by the U.K. Meteorological Office. But during the whole campaign, coincidences between the C-130 measurements and the SSM/I overpasses were rather scarce, and were not always located in cloudy areas. For the coincidence between the C-130 and SSM/I in clear sky conditions, we verified that our scheme does not predict liquid water. For these cases, the FSSP on the C-130 detected no cloud droplets, and the clear skies were confirmed by visual checks from the aircraft. These comparisons were performed for instance at 1007 UTC 4 June, when the C-130 underpassed the *F10* spacecraft. The C-130 measured no liquid water, and the SSM/I also predicted no liquid water. For the whole ASTEX period, only two situations were found to satisfy our selection criteria—that is, coincidence in cloudy areas with less than a 2-h difference between the SSM/I overpass and the measurement of cloud profile. For these two situations, on 19 and 22 June, the SSM/I-retrieved products are calculated in the area of the aircraft cloud profile measurements.

At 0810 UTC 19 June, the C-130 carried out a descent profile down through a solid stratocumulus sheet, from 850 up to 800 mb, for which the integrated cloud liquid water content was 0.39 kg m^{-2} (Fig. 8a). On this day, the *F11* spacecraft overpassed the Azores at 0723 UTC, and the corresponding SSM/I liquid water retrievals are displayed in Fig. 8b. The SSM/I liquid water field is spatially smooth, showing a band of rather dense cloud oriented northwest–southeast and surrounded by clearer areas. The ISCCP retrieval performed at 0900 UTC is also shown for comparison (Fig. 8c). The spatial structures of the SSM/I and ISCCP retrievals are consistent, with the ISCCP cloud band shifted slightly southwest as compared to the SSM/I retrieval, which is consistent with the northeasterly airflow covering the whole region in this period.

On 22 June, the C-130 passed through a sheet of marine stratocumulus at 1120 UTC. The measured cloud profile is noisy, with an LWP of 0.129 kg m^{-2} (Fig. 9a). The *F10* overpassing time in the area is 1048 UTC. The SSM/I retrieved liquid water field exhibits rather low liquid water content, with few distinct cloud patches in the area (Fig. 9b). The ISCCP estimations at 1200 UTC produce very similar LWP and cloud structures (Fig. 9c).

For these two situations, the SSM/I and ISCCP LWP fields are consistent with the direct cloud liquid measurements, given the range of uncertainty caused by the different sampling characteristics of the observing systems and enhanced by the time difference of the measurements.

For these two cases, the cloud liquid water retrievals are compared with other algorithms available in the literature (Figs. 8d and 9d). The algorithms of Alishouse et al. (1990b) are based on comparisons between SSM/I observations and a ground-based radiometer estimation of the liquid water path. The one we use in this study involves four channels (Table 4 in their paper). Weng and Grody (1995), Petty and Katsaros (1990), and Bauer and Schluessel (1993) derived their algorithms from radiative transfer simulation. Petty and Katsaros's algorithm used in this study relies upon the 37-GHz observations. In low stratus clouds and stratocumulus clouds formed in the marine oceanic atmosphere, the amount of liquid water is rather low. Although there is a high scatter in the diagrams, the overall agreement is better with Weng and Grody's algorithm, which proposes different algorithms depending on the range of liquid water contents in the scene, and should be better adapted for low liquid water content retrievals. Bauer and Schluessel (1993) were aware of a possible overestimation of their algorithms in the case of low liquid water, due to the difficulty of discriminating between a cloud-free situation and a thin cloud layer. Compared with their own SSM/I algorithm (which makes use of IR ancillary data),

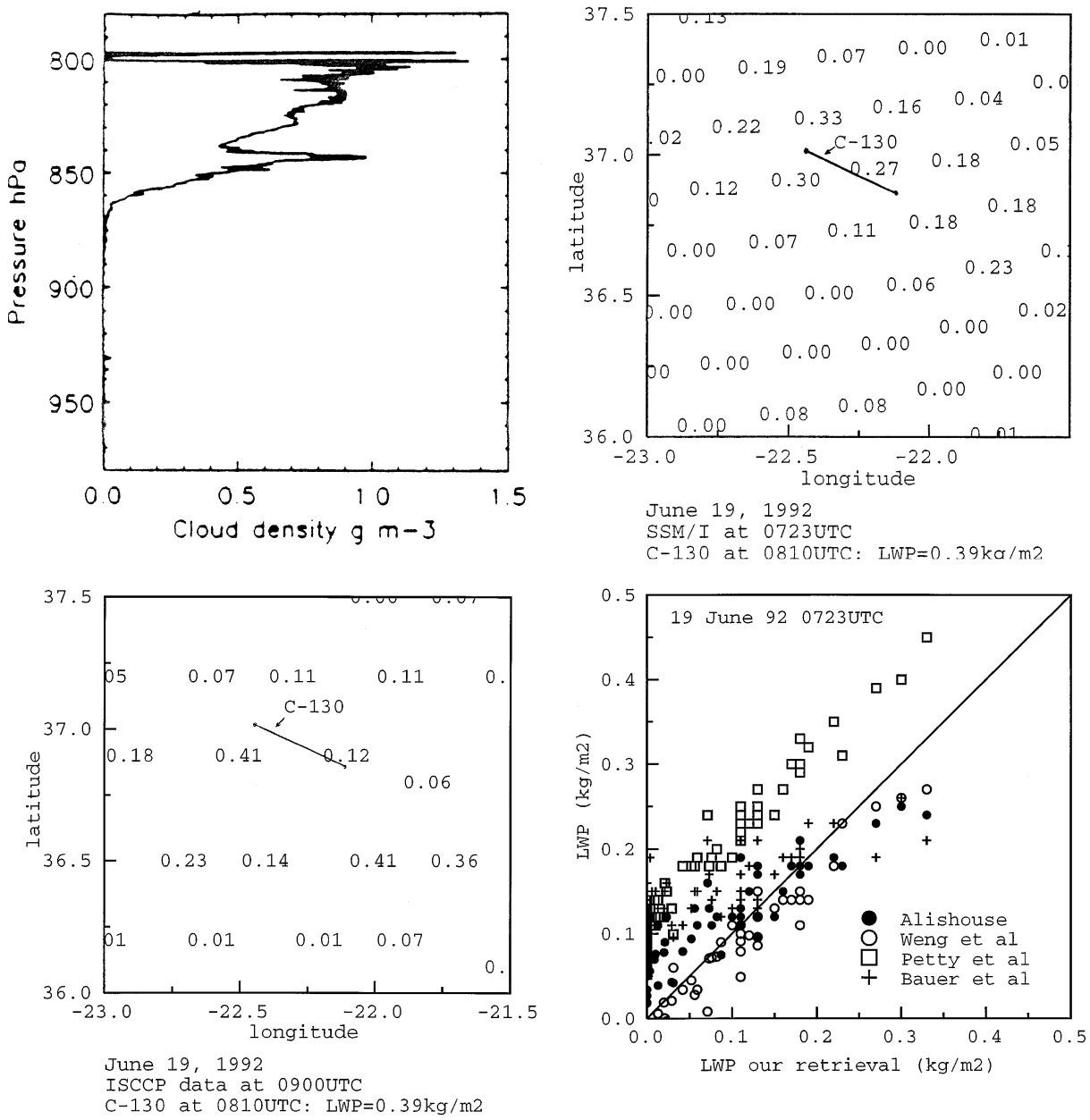

FIG. 8. For 19 June 1992, (a) the cloud profile measured by the Johnson–William probe onboard the C-130, (b) the SSM/I-retrieved cloud liquid water fields in the vicinity of the C-130 in situ cloud profile, (c) the ISCCP LWP estimation in the same area, and (d) comparison of several SSM/I LWP algorithms for this situation.

Liu and Curry (1993) also noticed an overestimation from Petty and Katsaros's approach in subtropical areas. The algorithm of Alishouse et al. yields a higher liquid water content on 19 June but a lower one on 22 June.

The SSM/I LWP retrievals have been compared to the ISCCP estimates for several situations throughout the ASTEX campaign. The maximum time difference tolerated between SSM/I overpassings and ISCCP observations is 1.5 h. The distance between ISCCP and SSM/I pixels is within 30 km. Based on optical measurements, the ISCCP estimates are not available at nighttime. A total of 2680 retrievals have been compared, 27% of which are cloud-free pixels detected by the ISCCP procedure. The mean and the standard deviation of the LWP estimates are presented in Table 2 for the ISCCP procedure and the SSM/I retrievals. Most regression-type SSM/I algorithms produce a certain number of negative LWP values. Including these negative values or setting them to zero can significantly change the average LWP values (see Table 2).

To estimate the ability of the SSM/I retrievals to discriminate between clear and cloudy conditions, the his-

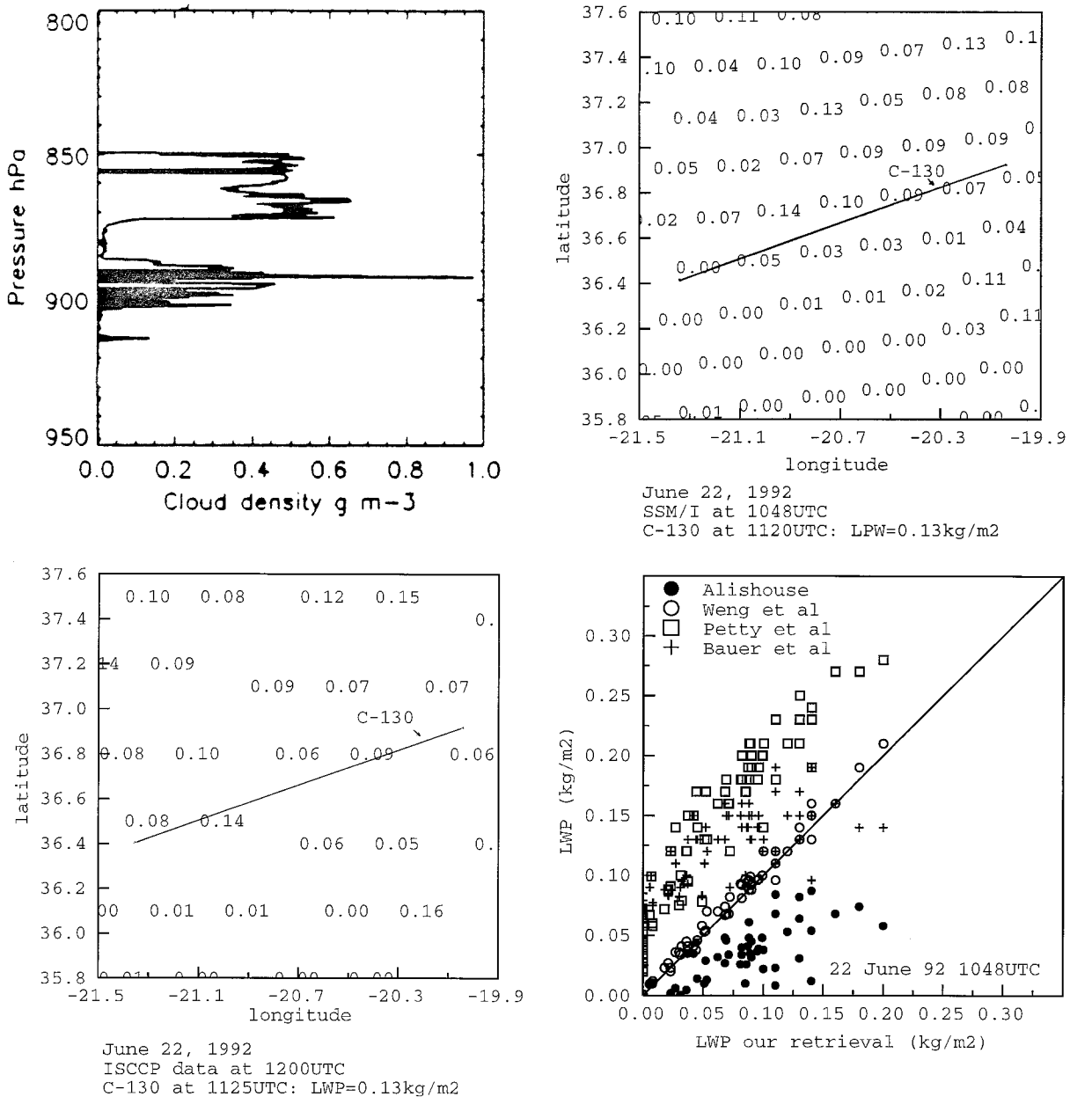

FIG. 9. Same as in Fig. 8 but for 22 June 1992.

TABLE 2. Mean and standard deviation of the LWP estimates (kg m^{-2}) for the ISCCP procedure and for the SSM/I retrievals. Both clear and cloudy pixels are included in the calculation; 2680 pixels are involved. The numbers on the left represent the results when including the negative LWP values; the values in parentheses on the right indicate the same quantities but when setting all the negative SSM/I LWP retrievals to zero (when negative values are present).

	ISCCP	Our retrieval	Weng et al. (1994)	Alishouse et al. (1990)	Petty et al. (1990)	Bauer et al. (1993)
Mean	0.03	0.02	0.01 (0.03)	0.03 (0.04)	0.10	0.12
Std. dev.	0.04	0.05	0.06 (0.05)	0.07 (0.06)	0.08	0.05

tograms of the retrieved SSM/I products are presented in Fig. 10, only for the pixels that are detected as clear sky by ISCCP. The corresponding histogram for Weng and Grody's algorithm is also presented—the negative LWP values have not been modified in this histogram. The corresponding mean LWP contents and their standard deviations are given in Table 3 for the four previously described statistical algorithms, along with our own method, first when including the negative LWP values and then when setting the LWP negative values to zero. The algorithm of Bauer and Schluessel (1993) and to a lesser extent the model of Petty and Katsaros

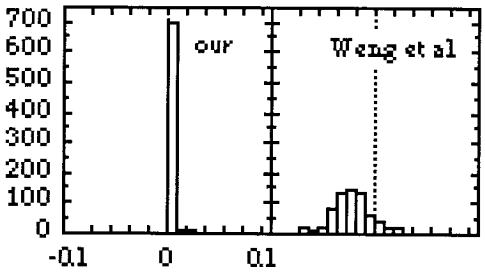

FIG. 10. Histograms of the SSM/I-retrieved LWP contents (kg m^{-2}) for cloud-free areas (as detected by the ISCCP procedure). The results for our retrieval are presented along with Weng and Grody's algorithms.

(1990) do not properly detect the clear-sky situations. When setting the LWP negative values to zero, our method and Weng and Grody's algorithm give very similar results—the clear-sky situations are correctly delineated.

In Fig. 11, for the situations that are considered cloudy by the ISCCP procedure, the histograms of the LWP contents derived from our method and Weng and Grody's algorithms are compared with the ISCCP estimates. Table 4 gives the statistical differences between the ISCCP and the SSM/I LWP products for all the algorithms previously considered. Bauer and Schluessel (1994) and Petty and Katsaros (1990) overestimated the cloud LWP, as compared to the ISCCP values. The other three SSM/I retrievals yield rather similar results. In Fig. 11, comparisons of the ISCCP histograms with the SSM/I histograms show that for many pixels the ISCCP procedure estimates low LWP clouds, while the SSM/I methods do not detect any cloud. The low sensitivity of the microwave to small values of LWP makes it difficult to separate clear and cloudy situations from microwave only. Nevertheless, the mean difference between ISCCP and our SSM/I retrieval tends to prove that, despite this handicap, microwave retrieval can yield LWPs that are comparable to the ISCCP estimates in this subtropical region.

5. Conclusions

In the framework of the ASTEX experiment, an inversion of the SSM/I observations involving ECMWF

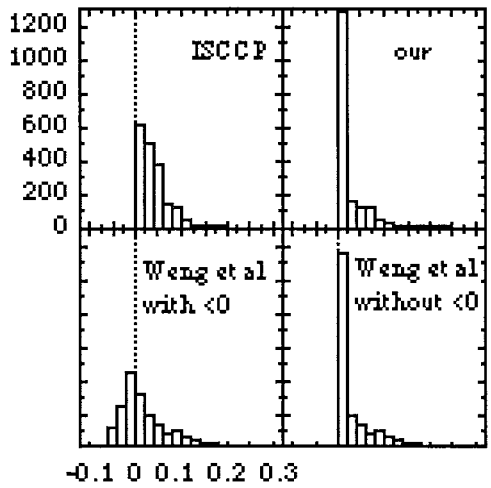

FIG. 11. Histograms of the retrieved LWP contents (kg m^{-2}) for the cloudy areas (as detected by the ISCCP procedure). The results are shown for ISCCP, our retrieval, and Weng and Grody's algorithm. For Weng and Grody's algorithm, the histograms presented are for when considering the negative values (on the left) and when setting all the negative values to zero (on the right).

a priori information is shown to simultaneously yield estimates of the surface wind speed, integrated water vapor, and liquid water contents that compare satisfactorily with the available in situ measurements. Without any arbitrary tuning of the radiative transfer model, unbiased geophysical parameters are derived. Contrary to the statistical algorithms, a quality criterion can be associated with each retrieval after the inversion process.

The ECMWF forecast provides the temperature profile, the structure of the humidity profile, and the sea surface temperature, along with a first guess of the wind speed and the water vapor content. It also enables the cloud to be defined in a manner consistent with the humidity and temperature structures, which avoids making use of global climatological values that can exhibit a large discrepancy with the real atmospheric state.

The water vapor estimations agree with the radiosonde observations, with a mean difference of -0.71 kg m^{-2} and an rms error of 2.26 kg m^{-2}, for the range of atmospheric conditions encountered during ASTEX (from 10 to 45 kg m^{-2} integrated water vapor contents). The wind speed SSM/I estimations and the point measurements compared well, with an rms error of 0.92 m s^{-1} and a mean value of -0.21 m s^{-1} for wind speeds

TABLE 3. Statistical differences between the ISCCP LWP estimate and the SSM/I retrieval (kg m^{-2}) for cloud-free areas, as detected by the ISCCP procedure. The numbers on the left represent the results when including the negative LWP values; the values in parentheses indicate the same quantities but when setting all the negative SSM/I LWP retrievals to zero (when negative values are present). Here, 730 clear-sky pixels are compared.

	Our retrieval	Weng et al. (1994)	Alishouse et al. (1990)	Petty et al. (1990)	Bauer et al. (1993)
Mean	0.00	0.02 (0.00)	0.00 (-0.01)	-0.04	-0.09
Std. dev.	0.01	0.03 (0.02)	0.03 (0.02)	0.03	0.02
rms	0.01	0.04 (0.02)	0.03 (0.02)	0.05	0.09

TABLE 4. Same as Table 3 but for cloudy conditions, as detected by the ISCCP procedure; 1950 cloudy pixels are compared.

	Our retrieval	Weng et al. (1994)	Alishouse et al. (1990)	Petty et al. (1990)	Bauer et al. (1993)
Mean	0.01	0.02 (0.01)	-0.01	-0.07	-0.08
Std. dev.	0.05	0.06 (0.05)	0.06	0.07	0.05
rms	0.06	0.06 (0.06)	0.06	0.09	0.09

up to 11 m s^{-1}. However, the sensitivity of the wind speed retrieval to the sea surface emissivity model is very critical and should be reexamined with care in the case of higher wind speeds. For the very few coincident observations between SSM/I overpasses and the C-130 aircraft flights, the SSM/I estimations are consistent with the aircraft cloud liquid water measurements. For the two studied situations, the SSM/I and the ISCCP estimations provide comparable LWP quantities and cloud spatial structures. For a larger number of meteorological situations throughout the campaign, the ISCCP LWP products and our estimates have also been compared. Our method properly diagnoses the clear-sky situations as delineated by the ISCCP procedure. Despite the difficulty of detecting the very low LWP clouds with SSM/I frequencies, our SSM/I retrievals and the ISCCP products are in good agreement in this subtropical area.

Comparison of model inversions against observed data is shown to be a useful mechanism for model validation. This procedure is adopted to test different radiative transfer models at SSM/I frequencies. At the end of the convergence process, the difference between the simulated and the observed radiances is a powerful tool to test the radiative transfer in use.

A similar variational retrieval has been used at ECMWF since March 1996 to retrieve surface wind speed, atmospheric moisture, and cloud liquid water path from SSM/I radiances over ocean (Phalippou 1996). This scheme runs on quasi-real time every day. At the moment, the retrieved products are used for monitoring the quality of the ECMWF analyses and forecasts and for comparisons with the National Environmental Satellite, Data, and Information Service regression algorithms. They are not yet used in the assimilation system.

Acknowledgments. The ASTEX campaign is a cooperative work involving several groups. The authors are grateful to A. Weill [Centre d'étude pour l'Environnement Terrestre et Planétaire (CETP), France] for access to the ASTEX data bank and to B. Syrett (The Pennsylvania State University) for providing the radiosounding data from the *Oceanus* and the *Malcolm Baldridge.* The C-130 cloud data were obtained by the Royal Air Force air and ground crew and the staff of the Meteorological Research Flight, and their efforts are gratefully acknowledged. Discussion with L. Eymard, A. Weill, and H. Dupuis from CETP were very helpful. The authors are grateful to B. Rossow (NASA/GISS, New York) for his comments on the manuscript. The help of Jennifer Miletta (NOAA Pacific Marine Environmental Laboratory, Washington) with the processing of the SSM/I data is also recognized with thanks. Three anonymous reviewers made helpful comments and suggestions for which the authors are grateful. This study has been partially supported by the Institut National des Sciences de l'Univers (France).

REFERENCES

Albrecht, B. A., C. S. Bretherton, D. W. Johnson, W. H. Shubert, and A. S. Frisch, 1995: The Atlantic Stratocumulus Transition Experiment—ASTEX. *Bull. Amer. Meteor. Soc.*, **76,** 889–904.

Alishouse, J. C., S. Snyder, J. Vongsathorn, and R. R. Ferraro, 1990a: Determination of oceanic total precipitable water from the SSM/I. *IEEE Trans. Geosci. Remote Sens.*, **28,** 811–816.

——, ——, E. R. Westwater, C. Swift, C. Ruf, S. Snyder, J. Vongsathorn, and R. R. Ferraro, 1990b: Determination of cloud liquid water content using the SSM/I. *IEEE Trans. Geosci. Remote Sens.*, **28,** 817–822.

Bauer, A., M. Godon, J. Carlier, Q. Ma, and R. H. Tipping, 1993: Absorption by H_2O and H_2O-N_2 mixture at 153GHz. *J. Quant. Spectrosc. Radiat. Transfer*, **50,** 463–475.

Bauer, P., and P. Schluessel, 1993: Rainfall, total water, ice water and water vapor above sea from polarized microwave simulations and Special Sensor Microwave/Imager data. *J. Geophys. Res.*, **98,** 20 737–20 759.

Bjerkaas, A. W., and F. W. Riedel, 1979: Proposed model for the elevation spectrum of a wind-roughened sea surface. Tech. Memo. JHU/APL TG 1328, 39 pp. [Available from Applied Physics Lab., Johns Hopkins University, Laurel, MD 20723.]

Cox, C., and W. Munk, 1954: Measurements of the roughness of the sea surface from photographs of the sun's glitter. *J. Opt. Soc. Amer.*, **44,** 838–850.

English, S., 1995: Airborne radiometric observations of cloud liquid water emission at 89 and 157GHz: Application to the retrieval of liquid water path. *Quart. J. Roy. Meteor. Soc.*, **121,** 1501–1524.

——, C. Guillou, C. Prigent, and D. C. Jones, 1994: Aircraft measurements of water vapour continuum absorption at millimetre wavelength. *Quart. J. Roy. Meteor. Soc.*, **120,** 603–625.

Eyre, J. R., 1989: Inversion of cloudy satellite sounding radiances by nonlinear optimal estimation. I: Theory and simulation for TOVS. *Quart. J. Roy. Meteor. Soc.*, **115,** 1001–1026.

——, G. A. Kelly, A. P. McNally, E. Anderson, and A. Persson, 1993: Assimilation of TOVS radiance information through one-dimensional variational analysis. *Quart. J. Roy. Meteor. Soc.*, **119,** 1427–1463.

Filiberti, M. A., L. Eymard, and B. Urban, 1994: Assimilation of satellite precipitable water in a meteorological forecast model. *Mon. Wea. Rev.*, **122,** 486–506.

Francis, C. R., D. P. Thomas, and E. P. L. Windsor, 1983: The evaluation of SMRR retrieval algorithms. *Satellite Microwave Remote Sensing*, T. D. Allen, Ed., Ellis Horwood, 481–498.

Gagarin, S. Y., and B. G. Kutusa, 1983: Influence of sea roughness and atmospheric inhomogeneities on microwave radiation of the atmosphere–ocean system. *IEEE J. Oceanic Eng.*, **8,** 62–70.

Goodberlet, M. A., C. T. Swift, and J. C. Wilkerson, 1989: Remote sensing of ocean surface winds with the Special Sensor Microwave/Imager. *J. Geophys. Res.*, **94,** 4547–4555.

Greenwald, T. J., G. L. Stephens, T. H. Vonder Haar, and D. L. Jackson, 1993: A physical retrieval of cloud liquid water over the global oceans using Special Sensor Microwave/Imager (SSM/I) observations. *J. Geophys. Res.*, **98,** 18 471–18 488.

Guillou, C., C. Prigent, S. English, and D. Jones, 1993: Gazeous absorption and sea surface emissivity models: Validation from aircraft measurements at millimeter waves. *Proc. IGARSS'93*, Tokyo, Japan, 1619–1621.

——, S. English, C. Prigent, and D. Jones, 1996: Passive microwave airborne measurements of the sea surface response at 89 and 157GHz. *J. Geophys. Res.*, **101,** 3775–3788.

Han, Y., J. Snider, and E. R. Westwater, 1994: Observations of water vapor by ground based microwave radiometers and Raman lidar. *J. Geophys. Res.*, **99,** 18 695–18 702.

Hollinger, J. P., 1991: DMSP Special Sensor Microwave/Imager. Vol. 2, Calibration/validation. Final Rep.

——, R. Lo, G. Poe, R. Savage, and J. Pierce, 1987: Special Sensor

Microwave/Imager user's guide. Naval Research Laboratory, 120 pp.

Karstens, U., C. Simmer, and E. Ruprecht, 1994: Remote sensing of cloud liquid water. *Meteor. Atmos. Phys.*, **54,** 157–171.

Klein, L. A., and C. T. Swift, 1977: An improved model for the dielectric constant of sea water at microwave frequencies. *IEEE Trans. Antennas Propag.*, **25,** 104–111.

Kuo, Y. H., Y. R. Guo, and E. R. Westwater, 1993: Assimilation of precipitable water measurements into a mesoscale numerical model. *Mon. Wea. Rev.*, **121,** 1215–1238.

Liebe, H. J., 1989: MPM—An atmospheric millimeter-wave propagation model. *Int. J. Infrared Millimeter Waves*, **10,** 631–650.

——, G. A. Hufford, and M. G. Cotton, 1993: Propagation modeling of moist air and suspended water/ice particles at frequencies below 1000GHz. *AGARD Specialist Meeting of the Electromagnetic Wave Propagation Panel*, Palma de Mallorca, Spain, 17–21.

Lin, B., and W. B. Rossow, 1994: Observations of cloud liquid water path over oceans: Optical and microwave remote sensing methods. *J. Geophys. Res.*, **99,** 20 907–20 927.

Liu, G., and J. A. Curry, 1993: Determination of characteristics features of cloud liquid water from satellite microwave measurements. *J. Geophys. Res.*, **98,** 5069–5092.

Ma, Q., and R. H. Tipping, 1990: Water vapor continuum in the millimeter spectral region. *J. Chem. Phys.*, **93,** 6127–6139.

Manabe, T., H. J. Liebe, and G. A. Hufford, 1987: Complex permittivity of water between 0 and 30 THz. *12th Int. Conf. on Infrared and Millimeter Waves*, Orlando, FL, IEEE, 229–230.

NAG, 1991: NAG FORTRAN library manual, mark 15. [Available from NAG Ltd., Oxford, United Kingdom.]

Petty, G., 1990: On the response of the Special Sensor Microwave Imager to the marine environment—Implications for atmospheric parameters retrievals. Ph.D. dissertation, University of Washington, 291 pp. [Available from University of Washington, Seattle, WA 98195.]

——, and K. B. Katsaros, 1990: New algorithms for the Special Sensor Microwave Imager. *Proc. Fifth Int. Conf. on Satellite Meteorology and Oceanography*, London, England, 247–251.

Phalippou, L., 1996: Variational retrieval of humidity profile, wind speed and cloud liquid water path with SSM/I: Potential for numerical weather prediction. *Quart. J. Roy. Meteor. Soc.*, **122,** 327–355.

Prigent, C., and P. Abba, 1990: Sea surface equivalent brightness temperature at millimeter wavelength. *Ann. Geophys.*, **8,** 627–634.

——, A. Sand, C. Klapisz, and Y. Lemaitre, 1994: Physical retrieval of liquid water contents in a North Atlantic cyclone using SSM/I data. *Quart. J. Roy. Meteor. Soc.*, **120,** 1179–1207.

Rodgers, C. D., 1976: Retrieval of atmospheric temperature and composition from remote measurements of thermal radiation. *Rev. Geophys. Space Phys.*, **14,** 609–624.

Rosenkranz, P. W., 1992: Absorption of microwaves by atmospheric gases. *Atmospheric Remote Sensing by Microwave Radiometry*, M. A. Janssen, Ed., Wiley-Interscience.

Rossow, W. B., and R. A. Schiffer, 1991: ISCCP cloud data products. *Bull. Amer. Meteor. Soc.*, **72,** 2–20.

Schluessel, P., and W. J. Emery, 1990: Atmospheric water vapour over the oceans from SSM/I measurements. *Int. J. Remote Sens.*, **11,** 753–766.

——, and H. Luthardt, 1991: Surface wind speed over the North Sea from Special Sensor Microwave/Imager observations. *J. Geophys. Res.*, **96,** 4845–4853.

Smith, R. N. B., 1990: A scheme for predicting layer clouds and their water content in a general circulation model. *Quart. J. Roy. Meteor. Soc.*, **116,** 435–460.

Stoeffelen, A., and D. Anderson, 1994: The ECMWF contribution to the characterisation, interpretation, calibration and validation of ERS-1 scatterometer backscatter measurements and wind, and their use in numerical weather prediction models, Final Rep. ESA Contract 90997/90/NL/BI.

Walter, S. J., 1992: The tropospheric microwave water vapor spectrum: Uncertainties for remote sensing. *Specialist Meeting on Microwave Radiometry and Remote Sensing Applications*, Boulder, CO, 203–210.

Weill, A., and Coauthors, 1995: SOFIA experiment during ASTEX. *Global Atmosphere and Ocean System*, Vol. 3, 355–395.

Weng, F., and N. Grody, 1995: Retrieval of liquid and ice water in atmosphere using Special Sensor Microwave Imager (SSM/I) data. *J. Geophys. Res.*, **100,** 25 535–25 551.

Wentz, F. J., 1975: A two-scale scattering model for foam-free sea microwave brightness temperatures. *J. Geophys. Res.*, **80,** 3441–3446.

——, 1992: Measurements of oceanic wind vector using satellite microwave radiometers. *IEEE Trans. Geosci. Remote Sens.*, **30,** 960–972.

Westwater, E. R., J. B. Snider, and M. J. Falls, 1990: Ground-based radiometric observations of atmospheric emission and attenuation at 20.6, 31.65, 90.0 GHz: A comparison of measurements and theory. *IEEE Trans. Antenna Propag.*, **38,** 1569–1580.

Wilheit, T. T., 1979: The effect of wind on the microwave emission from the ocean's surface at 37 GHz. *J. Geophys. Res.*, **84,** 4921–4926.

Wu, S. T., 1979: Oceanic whitecaps and sea state. *J. Phys. Oceanogr.*, **9,** 1064–1068.

——, and A. K. Fung, 1972: A noncoherent model for microwave emissions and backscattering from the sea surface. *J. Geophys. Res.*, **77,** 5917–5929.